Laser Physics, Vol. 13, No. 9, 2003, pp. 1196–1204.

Quantum-Orbit Analysis of Nonsequential Double Ionization

C. Figueira de Morisson Faria* and W. Becker

Max Born-Institut für nichtlineare Optik und Kurzzeitspektroskopie, Max Born-Str. 2A, D-12489 Berlin, Germany

e-mail: faria@mbi-berlin.de, wbecker@mbi-berlin.de

Received October 9, 2002

Abstract—The *S*-matrix element that embodies the rescattering scenario for nonsequential double ionization is analyzed in terms of the saddle-point approximation, which yields a decomposition of the transition amplitude in terms of electronic orbits. These describe an electron freed by ionization that removes the second electron in a laser-assisted recollision. The orbits come in pairs that nearly merge near the classical cutoffs. In the latter situation, the saddle-point approximation becomes insufficient and the uniform approximation must be used, which correctly yields the contribution of a pair of saddle points, near the cutoffs as well as away from them. The shortest two orbits are analyzed in detail, and the role of "slow-down collisions" within the model is assessed.

1. INTRODUCTION

Recent differential measurements of electron and/or ion momentum distributions, in the context of double ionization of rare gases in strong laser fields [1, 2], have shed more light on the physical mechanisms involved and highlighted the dominant role of recollisions [3] for nonsequential double ionization (NSDI). The recollision or rescattering picture is instrumental for high-order harmonic generation and high-order above-threshold ionization (for reviews, see [4–6]). Nonsequential double ionization adds another item to the list of options that are available to the recolliding electron. Exactly how the electron accomplishes this when it returns to its parent ion is still a matter of much debate. The crucial role of the recollision, however, appears to be a fact.

For nonsequential double ionization, this recollision scenario has recently been formulated quantum mechanically [7–13]. This approach invokes the strong-field approximation [14] and results in multidimensional integrals, which, for a zero-range potential, can be solved analytically up to one final quadrature [10]. For an arbitrary binding potential, such integrals can be solved either numerically [8, 9] or by means of a saddle-point approximation [11–13]. The latter, apart from considerably simplifying the computations involved, is very illuminating from the physical point of view. Indeed, the saddle-point method introduces the concept of "quantum orbits" [15]. These are closely related to classical orbits that describe an electron "born" through tunneling that subsequently propagates in the laser field and returns to its parent ion. They are complex to account for the process of tunneling. The transition amplitude is a coherent superposition of the contributions of the various quantum orbits, in the fashion of Feynman's path integral [16]. These methods have been widely used for the description of above-threshold ionization (ATI) and high-order harmonic generation (HHG).

Quantum orbits depend on the final state of the respective laser–atom process, that is, on the harmonic order for HHG or on the final momentum of the electron for ATI. For a specified final state, they naturally occur in pairs. The best-known example may be the "short orbit" and the "long orbit" in HHG [15]. When the final state is varied towards the classical cutoff, the two orbits of such a pair approach each other very closely [17]. They would actually coalesce if it were not for their imaginary parts. In this situation, the saddle-point approximation becomes unreliable or breaks down, since it treats individual saddle points as independent. This is detrimental to quantitative predictions and may introduce qualitative artifacts. Recently, this problem has been overcome, for above-threshold ionization, by a specific version of the uniform approximation [18, 19] tailored to the case of saddles occurring in pairs [20, 21]. It is superior to the commonly used saddle-point approximation, to which it reduces when the saddles are sufficiently far apart, and is hardly more complicated.

In this paper, we apply the saddle-point and the uniform approximations to NSDI by calculating the transition amplitude considered in [9–13]. The approach is closely related to that of [11–13]. However, we evaluate the pertinent quantum orbits purely numerically, avoiding approximations that are inherent in the semi-analytical treatment employed in these references. Moreover, we make use of the uniform approximation, which for NSDI is more important than for ATI and HHG: While for HHG and ATI the saddle-point approximation produces quantitatively accurate results except in comparatively narrow regions around the classical cutoffs, this is not so if one is interested in the electron-momentum distributions that have recently been recorded in NSDI. These measurements yield, for example, the distribu-

*Present address: Quantum Optics Group, Institut für theoretische, Physik Universität Hannover, Appelstr, 2, 30167 Hanover, Germany.

tion of the momenta of the two electrons parallel to the laser field regardless of the transverse components, which are summed over. Since, for fixed longitudinal momentum, the spectrum exhibits a cutoff with respect to the transverse momentum, one is confronted with a cutoff situation throughout the entire range of longitudinal momenta. Hence, the standard saddle-point approximation produces unreliable results everywhere.

The paper is organized as follows. In Section 2, we write down the transition amplitude for NSDI in the strong-field approximation. The amplitude is evaluated in Section 3 by means of the saddle-point and the uniform approximations. In Section 4, we provide an extensive discussion of the most relevant pair of the shortest quantum orbits and compare the two approximations for simple cases. In the classically allowed regime, we find that recollisions with and against the force of the laser field are of comparable significance. We summarize the paper and discuss the advantages and shortcomings of its framework in Section 5. In the following sections, we use atomic units throughout.

2. THE TRANSITION AMPLITUDE

The transition amplitude for nonsequential double ionization in the presence of a strong laser field that describes the inelastic-rescattering scenario is given by

$$M_{\mathbf{p}} = -\int_{-\infty}^{\infty} dt \int_{-\infty}^{t} dt' \langle \psi_{\mathbf{p}}^{(\mathrm{Vv})}(t) | V_{12} U_1^{(\mathrm{Vv})}(t, t') V_1 | \psi_0(t') \rangle, \quad (1)$$

where V_n and $U_n^{(\mathrm{Vv})}(t, t')$ denote the atomic binding potential and the Volkov time-evolution operator acting on the nth electron ($n = 1, 2$), respectively, and V_{12} is the electron–electron interaction, by which the returning electron dislodges the bound electron. The above-stated amplitude can be understood as follows. Initially, both electrons are bound and the atom is in its ground state $|\psi_0(t')\rangle \equiv |\psi_0^{(1)}(t')\rangle \otimes |\psi_0^{(2)}(t')\rangle$, with $|\psi_0^{(n)}(t')\rangle = \exp(i|E_{0n}|t')|\psi_0^{(n)}\rangle$. At the time t', the first electron is set free by ionization, whereas the second electron remains bound. The first electron propagates in the continuum from t' up to the later time t, when it recollides with its parent ion and liberates the second electron. The final electron state then is $|\psi_{\mathbf{p}}^{(\mathrm{Vv})}(t)\rangle \equiv |\psi_{\mathbf{p}_1}^{(\mathrm{Vv})}(t)\rangle \otimes |\psi_{\mathbf{p}_2}^{(\mathrm{Vv})}(t)\rangle$, i.e., both electrons are in Volkov states with asymptotic momenta $\mathbf{p}_1$ and $\mathbf{p}_2$, and their Coulomb repulsion is neglected. Here and below, we make use of the notation $\mathbf{p} \equiv (\mathbf{p}_1, \mathbf{p}_2)$. Equation (1) has been derived [7, 8] within the framework known as the strong-field approximation (SFA). This approximation mainly consists in neglecting the binding potential during the propagation of the electron in the continuum and the laser field as long as the electron is bound. The electron–electron interaction V_{12} is treated in the Born approximation.

Using the expansion of $U^{(\mathrm{Vv})}(t, t')$ in terms of Volkov states, Eq. (1) can be written as

$$M_{\mathbf{p}} = -\int_{-\infty}^{\infty} dt \int_{-\infty}^{t} dt' \int d^3\mathbf{k} V_{\mathbf{pk}} V_{\mathbf{k}0} \exp[iS_{\mathbf{p}}(t, t', \mathbf{k})] \quad (2)$$

with the action

$$S_{\mathbf{p}}(t, t', \mathbf{k}) = -\frac{1}{2}\left[\sum_{n=1}^{2} \int_{t}^{\infty} d\tau [\mathbf{p}_n + \mathbf{A}(\tau)]^2 + \int_{t'}^{t} d\tau [\mathbf{k} + \mathbf{A}(\tau)]^2\right] + |E_{01}|t' + |E_{02}|t, \quad (3)$$

where $\mathbf{A}(t)$ and $\mathbf{k}$ denote the vector potential of the laser field and the intermediate momentum, respectively. The potentials enter via their form factors [11–13]

$$V_{\mathbf{pk}} = \langle \mathbf{p}_2 + \mathbf{A}(t), \mathbf{p}_1 + \mathbf{A}(t) | V_{12} | \mathbf{k} + \mathbf{A}(t), \psi_0^{(2)} \rangle \quad (4)$$

and

$$V_{\mathbf{k}0} = \langle \mathbf{k} + \mathbf{A}(t') | V_1 | \psi_0^{(1)} \rangle. \quad (5)$$

For contact potentials, such form factors are constant.

3. THE SADDLE-POINT AND THE UNIFORM APPROXIMATION

For sufficiently high intensity and low frequency, the five-dimensional integration in the amplitude (2) can be carried out by the method of steepest descent [11–13]. To this end, those values of the integration variables $\mathbf{k}$, t, and t' are determined for which the action (3) is stationary. This yields the saddle-point equations

$$[\mathbf{k} + \mathbf{A}(t')]^2 = -2|E_{01}|, \quad (6a)$$

$$\sum_{n=1}^{2} [\mathbf{p}_n + \mathbf{A}(t)]^2 = [\mathbf{k} + \mathbf{A}(t)]^2 - 2|E_{02}|, \quad (6b)$$

$$\int_{t'}^{t} d\tau [\mathbf{k} + \mathbf{A}(\tau)] = 0. \quad (6c)$$

Equations (6a) and (6b) correspond to energy conservation at the ionization and rescattering times, respectively, while Eq. (6c) specifies the intermediate electron momentum $\mathbf{k}$. One should note that Eq. (6b) describes inelastic rescattering. Indeed, the returning first electron donates part of its kinetic energy to free the second electron. For $E_{01} \neq 0$, the first equation has no real solutions. Hence, t, t', and $\mathbf{k}$ all become complex.

The approximation where the binding energy of the first electron is neglected, viz., $E_{01} = 0$, is often referred

to as the simple-man model. In this limit, the electron does not have to tunnel. As required by Eq. (6a), it starts its orbit in the presence of the field with zero velocity. Double ionization can proceed classically, provided the final momenta of the two electrons are classically accessible. If we decompose the final momenta in terms of their components $p_{n\parallel}$ and $\mathbf{p}_{n\perp}$ parallel and perpendicular to the polarization axis of the laser field, Eq. (6b) can be rewritten as

$$\sum_{n=1}^{2}[p_{n\parallel}+A(t)]^2 = [\mathbf{k}+\mathbf{A}(t)]^2 - 2|E_{02}| - \sum_{n=1}^{2}\mathbf{p}_{n\perp}^2. \tag{7}$$

This shows that, in effect, the transverse kinetic energies increase the second ionization potential $|E_{02}|$. A necessary condition for a classical pathway to double ionization is that the right-hand side of Eq. (7) be positive. It is definitely negative if

$$(\mathbf{p}_{1\perp}^2 + \mathbf{p}_{2\perp}^2)/2 + |E_{02}| > 3.17U_P, \tag{8}$$

where $U_P = \langle \mathbf{A}(t)^2\rangle_t/2$ is the ponderomotive energy of the laser field. If Eq. (7) is not satisfied, only quantum mechanics allows liberation of the second electron, whereby tunneling or multiphoton transfer assists the recolliding first electron.

In general, the saddle-point equations (6) are solved numerically. Their solutions then determine the transition amplitude

$$M_{\mathbf{p}}^{(\mathrm{SPA})} = \sum_s A_{\mathbf{p}s}\exp(iS_{\mathbf{p}s}), \tag{9}$$

with

$$S_{\mathbf{p}s} = S_{\mathbf{p}}(t_s, t_s', \mathbf{k}_s), \tag{10}$$

$$A_{\mathbf{p}\mathbf{k}s} = (2\pi i)^{5/2}\frac{V_{\mathbf{p}\mathbf{k}_s}V_{\mathbf{k}_s 0}}{\sqrt{\det S_{\mathbf{p}}''(t, t', \mathbf{k})|_s}}, \tag{11}$$

where the index s runs over the relevant saddle points and $S_{\mathbf{p}}''$ denotes the five-dimensional matrix of the second derivatives of the action (3) with respect to t, t', and $\mathbf{k}$.

In practice, we adopt a slightly different procedure, which considerably simplifies the computations involved. We first evaluate the three-dimensional integral over $\mathbf{k}$ in the transition amplitude (2) by saddle-point integration, which amounts to replacing

$$\mathbf{k} \longrightarrow \mathbf{k}(t, t') = -\frac{1}{t-t'}\int_{t'}^{t}A(\tau)d\tau \tag{12}$$

and $S_{\mathbf{p}}(t, t') \longrightarrow S_{\mathbf{p}}(t, t', \mathbf{k}(t, t'))$. Then, we again use the saddle-point approximation to compute the two-dimensional integral over t and t'. This results in the amplitude (9), where the actions and amplitudes are now computed by

$$S_{\mathbf{p}s} = S_{\mathbf{p}}(t_s, t_s'), \tag{13}$$

$$A_{\mathbf{p}\mathbf{k}s} = (2\pi i)^{5/2}\frac{V_{\mathbf{p}\mathbf{k}(t_s, t_s')}V_{\mathbf{k}(t_s, t_s')0}}{\sqrt{(t_s - t_s')^3\det S_{\mathbf{p}}''(t, t')|_s}} \tag{14}$$

and $\det S_{\mathbf{p}}''(t, t')|_s$ denotes the determinant of the second derivatives of the action with respect to t and t'. The action then reads

$$S_{\mathbf{p}}(t, t') = \frac{1}{2}\left\{\sum_{n=1}^{2}\mathbf{p}_n^2 t + \frac{1}{(t-t')}[F_1(t) - F_1(t')]^2 + 2\sum_{n=1}^{2}p_{n\parallel}F_1(t) + F_2(t) + F_2(t')\right\} + |E_{01}|t' + |E_{02}|t \tag{15}$$

with the indefinite integrals

$$F_1(t) = \int^t A(t)dt, \tag{16}$$

and

$$F_2(t) = \int^t A^2(t)dt. \tag{17}$$

The saddle-point approximation can only be applied when the saddle points are well separated, which is not the case near the boundary of the classically allowed region pertinent to a given pair of orbits. Outside of the classically allowed region, the pair of orbits continues to exist but their imaginary parts rapidly increase. The contribution of one of the two orbits then has to be dropped from the transition amplitude (9), as it would generate an exponentially increasing contribution [17]. The formal justification of discarding this contribution is as follows. The original integration contour for the amplitude (1) is the five-dimensional real (t, t', $\mathbf{k}$) hyperplane. In the process of the saddle-point approximation, this contour is deformed into a complex hyperplane that encompasses the relevant complex saddle points. At some point along the way from the classically allowed into the classically forbidden region the contour can no longer be deformed such that it passes through *both* saddle points. One of the two saddle points, the one that would generate the exponentially increasing contribution, will come to lie off the contour. This qualitative change in the contour of integration is known as the "Stokes transition" [19]. For a pair of trajectories, denoted by i and j, this point corresponds to a value of $\mathbf{p}$ such that

$$\mathrm{Re}\,S_{\mathbf{p}}(t_i, t_i', \mathbf{k}_i) = \mathrm{Re}\,S_{\mathbf{p}}(t_j, t_j', \mathbf{k}_j). \tag{18}$$

Usually, this is very close to the boundary of the classically allowed region. Discarding then the unphysical saddle point leads to a cusp in the transition amplitude.

For high-order ATI and for HHG, the classical cutoffs occur at the well-known energies $10U_P$ and $|E_0| + 3.17U_P$, respectively. For NSDI, in addition to such a maximal energy, there is also a minimal classically allowed energy. The region delimited by these two boundaries depends on the driving field, on the transverse momenta of both electrons, and on the ionization potentials $|E_{01}|$ and $|E_{02}|$.

Thus, one needs a method that also works when the saddle points *i* and *j* that make up a pair nearly coalesce and that yields a smooth transition from the classically allowed into the classically forbidden region. This is afforded by the uniform approximation, which was successfully applied in [21] for ATI. For a detailed discussion, we refer the reader to [18, 20, 21]; here, we will be content with reproducing the result.

For any pair of trajectories denoted by *i* and *j*, in the classically allowed region, the contribution of this pair to the transition amplitude is given by

$$\begin{aligned} M_{i+j} &= \sqrt{2\pi\Delta S/3}\exp(i\bar{S} + i\pi/4) \\ &\times\{\Delta A[J_{1/3}(\Delta S) + J_{-1/3}(\Delta S)] \\ &+ \bar{A}[J_{2/3}(\Delta S) - J_{2/3}(\Delta S)]\}, \end{aligned} \tag{19}$$

where

$$\begin{aligned} \Delta S &= (S_i - S_j)/2, \quad \bar{S} = (S_i + S_j)/2, \\ \Delta A &= (A_i - iA_j)/2, \quad \bar{A} = (iA_i - A_j)/2 \end{aligned} \tag{20}$$

are determined by the actions and the prefactors evaluated at the individual saddle points. For large values of ΔS, i.e., when the two saddle points are well separated, the uniform approximation (19) approaches the saddle-point approximation (9). This can be checked with the help of the asymptotic behavior

$$J_\nu(z) \sim \left(\frac{2}{\pi z}\right)^{1/2}\cos(z - \nu\pi/2 - \pi/4) \tag{21}$$

of the Bessel functions for large *z*. Note that the only input that enters the uniform approximation (19) consists of the actions S_i and the associated prefactors A_i, which were required for the saddle-point approximation. No additional information, such as higher derivatives of the action, is needed.

In the classically forbidden region, where one of the saddles is bypassed by the contour, one must take an appropriate functional branch of the Bessel functions, which will automatically be selected by requiring a smooth functional behavior at a Stokes transition [19]. The corresponding transition amplitude is then given by

$$\begin{aligned} M_{i+j} &= \sqrt{2i\Delta S/\pi}\exp(i\bar{S}) \\ &\times[\bar{A}K_{1/3}(-i\Delta S) + i\Delta A K_{2/3}(-i\Delta S)]. \end{aligned} \tag{22}$$

Using the asymptotic expansion

$$K_\nu(z) \sim \left(\frac{\pi}{2z}\right)^{1/2}\exp(-z), \tag{23}$$

one may again check that the saddle-point approximation is recovered for large ΔS and that it contains the contribution of only one saddle, viz., the saddle *i*. Equations (19) and (22) should be matched at the Stokes transitions. For nonsequential double ionization, there exist two energies for which such transitions occur, which will be referred to as the upper and the lower cutoff. Their energy positions roughly coincide with the maximum and minimum classically allowed momenta, respectively, and thus mark the boundary between the classically allowed and forbidden domains.

4. QUANTUM ORBITS AND ELECTRON-MOMENTUM DISTRIBUTIONS

In the evaluation of the *S* matrix, either by the saddle-point approximation or by the uniform approximation, the first step consists in finding the solutions of the saddle-point equations (6). We shall consider the monochromatic linearly polarized field

$$A(t) = -A_0\cos\omega t. \tag{24}$$

In this case, Eqs. (6) reduce to, respectively,

$$k/A_0 - \cos\omega t' = i\epsilon_\gamma\gamma_1, \tag{25a}$$

$$k/A_0 - \cos\omega t = \epsilon_\delta\delta(t), \tag{25b}$$

$$k/A_0 = \frac{1}{\omega(t - t')}(\sin\omega t - \sin\omega t'), \tag{25c}$$

where

$$\gamma_1 = \sqrt{\frac{|E_{01}|}{2U_p}} \tag{26}$$

is the Keldysh parameter corresponding to the ionization of the first electron and

$$\begin{aligned} \delta^2(t) &= \sum_{n=1}^{2}\left[\frac{p_{n\|}}{2\sqrt{U_p}} - \cos\omega t\right]^2 \\ &+ \sum_{n=1}^{2}\left(\frac{\mathbf{p}_{n\perp}}{2\sqrt{U_p}}\right)^2 + \frac{|E_{02}|}{2U_p}. \end{aligned} \tag{27}$$

The quantities ϵ_i ($i = \gamma, \delta$) identify the signs of the square roots, so that $\epsilon_i = \pm 1$. Eliminating *k*, we can rewrite the saddle-point equations as

$$\cos\omega t' = \cos\omega t + i\epsilon_\gamma\gamma_1 - \epsilon_\delta\delta(t) \equiv \xi, \tag{28}$$

$$\begin{aligned} &\sin\omega t - \epsilon_\xi\sqrt{1 - \xi^2} \\ &-(\omega t - \arccos\xi)(\cos\omega t - \epsilon_\delta\delta(t)) = 0. \end{aligned} \tag{29}$$

Equation (29) has to be solved numerically for the recollision time t with $\xi \equiv \xi(t)$ as defined in Eq. (28). Thereafter, the ionization time t' is determined from Eq. (28). The signs ϵ_i of the various square roots and the multivaluedness of the arccos in Eq. (29) generate an infinite number of solutions [17, 22]. Here, we will be satisfied with considering the pair of solutions having the shortest travel times $\mathrm{Re}(t - t')$. These are obtained by taking $-\epsilon_\gamma = \epsilon_\delta = \epsilon_\xi = 1$ and the principal branch of the arccos both in Eq. (29) and in inverting Eq. (28). Except at channel closings, these two make the dominant contributions [22].

In Fig. 1, the real and imaginary parts of the pair (t, t') obtained for the shortest pair of trajectories are displayed as functions of $p_\parallel$. The results shown are for equal longitudinal momenta for both particles (i.e., $p_{1\parallel} = p_{2\parallel} \equiv p_\parallel$) and for various fixed transverse momenta $p_{1\perp}$ and $p_{2\perp}$. In the classical (simple-man) limit where $E_{01} = 0$ (or $\gamma_1 = 0$) and for classically allowed momenta [cf. Eq. (7)], for fixed $p_\parallel$ and $p_{n\perp}$ ($n = 1, 2$) there exist two sets of times that are solutions of the saddle-point equations (6) [or (25)], which merge into one at the minimal and maximal classically allowed momenta. These times correspond to two possible trajectories for the electron, one with a shorter and the other with a longer travel time between ionization and recollision. For $E_{01} \neq 0$, the pairs (t, t') computed from the saddle-point equations have a similar behavior inside the classically allowed regime. They are, however, complex: they have continuations into the classically forbidden domain and they do not exactly coalesce near the classical cutoffs. Well inside the classically allowed region, the real parts of the emission and return times are largely independent of E_{01}.

Figure 1, even though it illustrates only the contributions of the two shortest orbits, contains a lot of information about the recollision model. For example, we can immediately read off the classically allowed domain of p for given $p_\perp$: in panel (d), the return time t is almost real in this regime, which indicates that the recollision dynamics can largely be envisioned in classical terms. Panel (b) shows that the real parts of the return times strongly depend on the momenta. In the classical domain, we recognize the long and the short orbit. Except for small momenta $p_\parallel$, the return times $\mathrm{Re}\,\omega t$ of the long orbit all exceed 2π, while those of the short orbit are below this value. Hence, an electron on a long orbit returns to the ion against the force of the electric field of the laser (in the language of [23], this is a slow-down collision), while an electron on a short orbit is accelerated by the field into the collision. Panel (a) shows that electrons on the long orbits start earlier than those on the short orbits. At these earlier times, the field is closer to its maximum and, consequently, tunneling is easier. This is reflected in panel (c), which shows that the imaginary part of the earlier start times is smaller than that of the later start times. This will give a slight advantage to the electron that starts earlier, which dislodges the second electron in a slow-down collision.

The panels also illustrate that the largest transverse momenta that we consider, viz., $(p_{\perp 1}, p_{\perp 2}) = (1.2, 2.0)$, are well outside of the classically allowed domain regardless of the value of $p_\parallel$. This can also be checked from Eq. (8). For these large transverse momenta, panels (b) and (d) show that the return times of the two orbits are almost complex conjugate to each other.

Outside the classically allowed region, for large momenta $p_\parallel$, the real parts of the return times ωt are almost independent of $p_\parallel$ and very close to 2π. At this time, the laser electric field is zero. An electron released at this time in the field with zero velocity acquires the largest drift momentum possible. According to the classical simple-man model, the corresponding start time is $\mathrm{Re}\,\omega t' \approx 1.8$, and, indeed, this is where the start times are concentrated (cf. panel (a)). It is interesting to observe that the start time that classically yields the highest possible return energy of $3.17U_P$ is $\omega t'_{\max} = 2.06 \mathrel{\hat{=}} 118°$. An electron that is to contribute to the nonclassical region for large momenta has to make a tough decision: either to take advantage of the highest possible energy of $3.17U_p$ for the inelastic collision or to make sure that the recollision takes place at the time when the field provides the largest drift momentum. It chooses the latter option. This is in spite of the fact that a nonzero electric field at the time of return would make it easier for the bound electron to escape [24], by tunneling or multiphoton absorption assisted by the returning first electron. The consequences of this barrier reduction are not as significant in three spatial dimensions as they are in one [25]. On the other hand, at the start time $\mathrm{Re}\,\omega t' \approx 1.8$, which the first electron actually chooses, the tunneling proceeds at a slightly higher rate than at $\omega t'_{\max} = 2.06$. Outside the classically allowed region, for small momenta $p_\parallel$, panel (b) displays return times around $\mathrm{Re}\,\omega t = 3\pi/2$, which give rise to a drift momentum of zero.

The curves traced out by the saddle points in the complex plane are exhibited in panels (e) and (f). The classical cutoffs for large momentum are easily recognized by the fact that the curves corresponding to the two orbits approach each other closely for these momenta. The corresponding cutoffs for low momenta are less pronounced.

The transition probability computed from the saddle-point amplitude (9), using such pairs, is shown in Fig. 2 for several fixed values of the transverse momenta. The calculation is done for the case where both the binding potential of the first electron and the electron–electron interaction are modeled by contact potentials such that the corresponding form factors (4) and (5) are constants. We take into account the pair of quantum orbits with the shortest excursion times. Such a pair already gives the main features of the corresponding momentum distributions [11]. The figure dis-

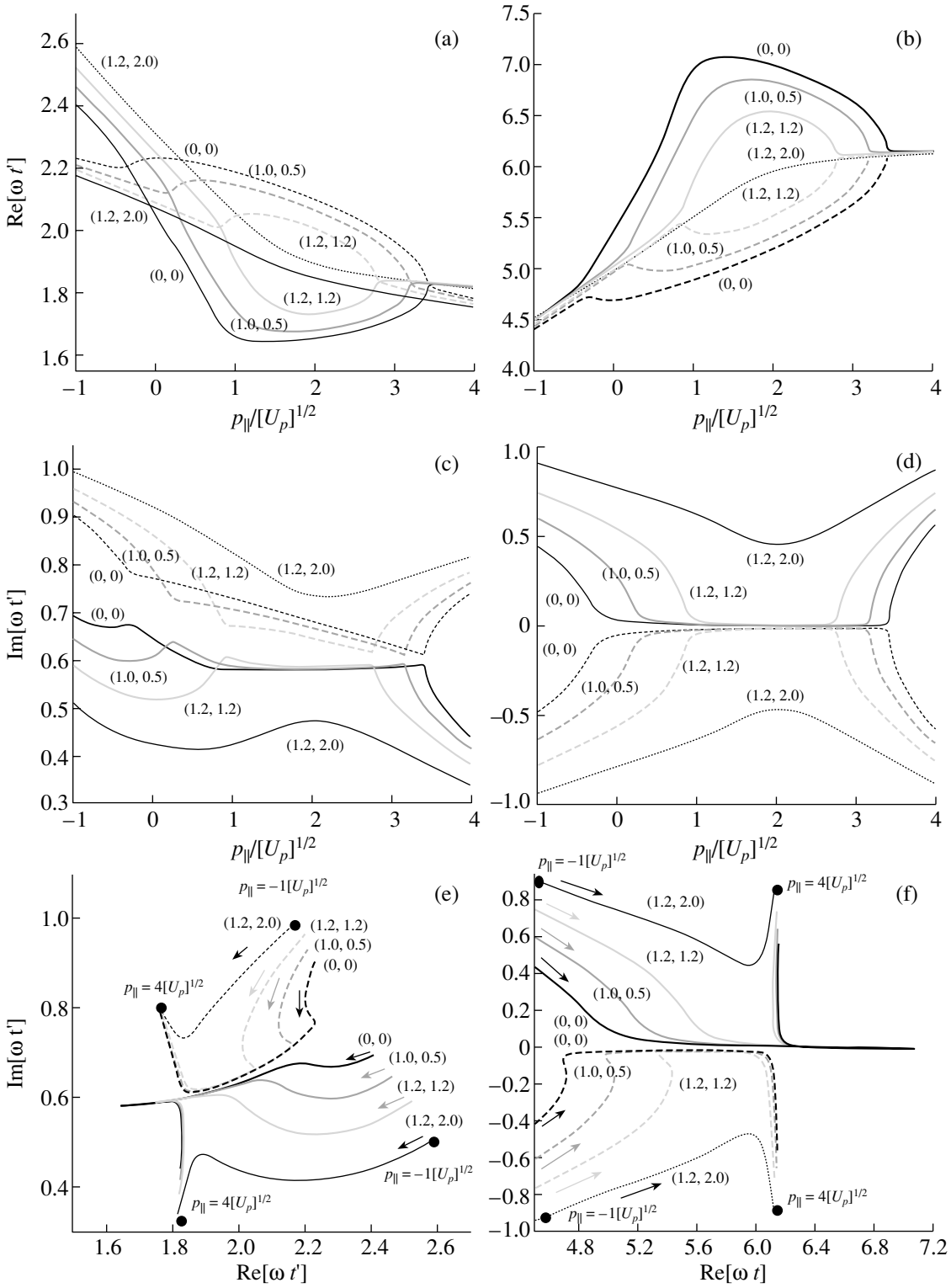

Fig. 1. Real and imaginary parts of start (first column) and return times (second column) determined by the saddle point equations for nonsequential double ionization in a monochromatic linearly polarized field of frequency ω = 0.0551 a.u. and ponderomotive energy U_p = 1.2 a.u., equal longitudinal momenta and several transverse momenta, for a monochromatic linearly polarized field, together with the respective saddles in the complex plane. The ionization potentials for the neutral atom and singly ionized case are given by $|E_{01}|$ = 0.9 a.u. and $|E_{02}|$ = 1.51 a.u., respectively, and correspond to neon. The numbers in the figure give the transverse momenta ($p_{1\perp}$, $p_{2\perp}$) in units of $\sqrt{U_p}$. The saddle which must be discarded beyond the cutoffs is given by the dashed lines. The arrows in the lowest part of the figure indicate the direction of increasing parallel momenta $p_\parallel$.

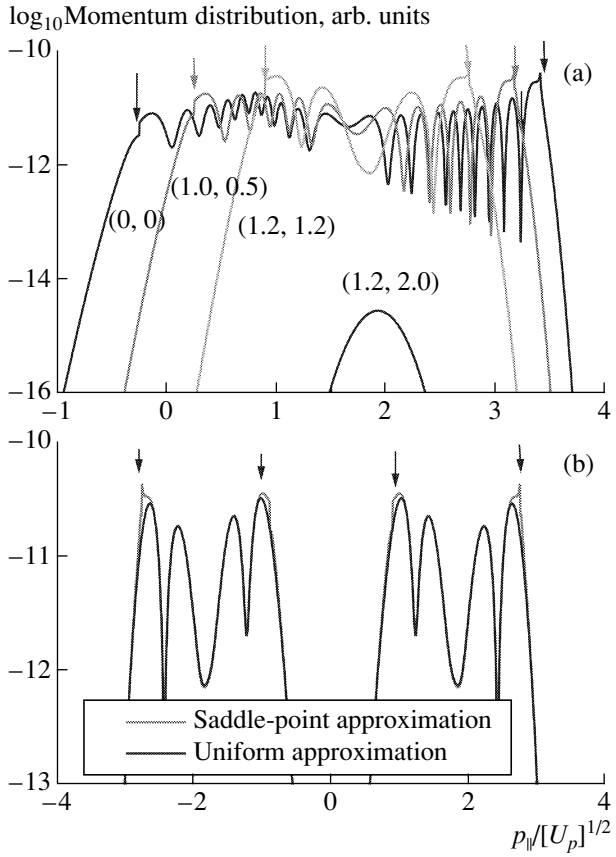

Fig. 2. Nonsequential double ionization yield $|M|^2$ computed with the saddle-point and uniform approximations as functions of the longitudinal momentum $p_\parallel$ for the same field and atomic parameters as in the previous figure and fixed transverse momenta. The Stokes transitions, which roughly coincide with the transition from the classically allowed to the classically forbidden energy regions, are marked with arrows. Part (a) gives only the right peak, whereas part (b) takes into account the left peak, which is originated by quantum orbits whose emission and return times are shifted in half a field cycle. The numbers in part (a) give the transverse momenta $(p_{1\perp}, p_{2\perp})$ in units of $\sqrt{U_p}$. In part (b), $(p_{1\perp}, p_{2\perp}) = (1.2\sqrt{U_p}, 1.2\sqrt{U_p})$.

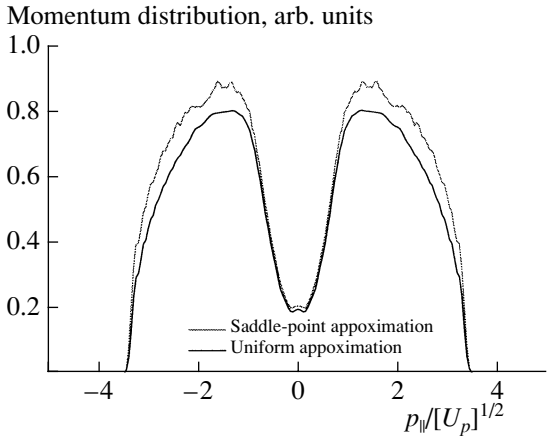

Fig. 3. Nonsequential double ionization yield $|M|^2$ computed with the saddle-point and uniform approximations as functions of the longitudinal momentum $p_\parallel$ for the same field and atomic parameters as in the previous figures summed over the transverse momentum. The yield is given in a linear scale.

plays several oscillations in the classically allowed region, followed by an exponentially decreasing yield beyond the classical cutoffs. Notice that the contribution of the classically forbidden transverse momenta $(p_{\perp 1}, p_{\perp 2}) = (1.2, 2.0)$ is concentrated around $p_\parallel \approx 1.9\sqrt{U_P}$, which is the value predicted by the classical simple-man model, whether above or below the threshold (8).

A small, but prominent, feature of the results obtained by the saddle-point approximation is the cusps near the cutoff energies, which are clear signs that this approximation breaks down. They come from the fact that, in the saddle-point approximation, the quantum orbit whose contribution to the yield diverges beyond the classically allowed region has to be discarded after the cutoff, which generates a discontinuity. Figure 2b shows that these artifacts are completely eliminated by the uniform approximation. At first sight, this improvement does not seem to influence the yield significantly, since the discrepancies between the saddle-point and the uniform approximation are restricted to a very narrow energy interval near the cutoffs. For transverse momenta outside of the classically allowed region, we only took into account the one saddle whose contribution decreases exponentially for large momenta.

For a periodic laser field (with period T) whose vector potential obeys $\mathbf{A}(t + T/2) = -\mathbf{A}(t)$, the momentum distributions are symmetric upon $\mathbf{p} \longrightarrow -\mathbf{p}$. In terms of quantum orbits, the latter symmetry is realized by the contributions of those orbits whose start and return times are shifted by half a period of the driving field. This has been used in the computation of the left-hand part of Fig. 2b.

Several experiments have recorded distributions of the momentum components parallel to the laser field of the two electrons freed in double ionization [1, 2]. Typically, in these data the transverse momenta are integrated over. In Fig. 3, we present such a distribution along the diagonal of the $(p_{\parallel 1}, p_{\parallel 2})$ plane so that $p_{\parallel 1} = p_{\parallel 2} \equiv p_\parallel$. The integration averages out the oscillations in the classically allowed region that are so dominant in Fig. 2. Moreover, it produces pronounced maxima, as they are characteristic of the experimental data [1, 2]. In our case, since we chose a contact potential to describe the electron–electron interaction, the maxima come to lie near $p_{1\parallel} = p_{2\parallel} = \pm 2\sqrt{U_p}$.

Figure 3 again shows a comparison of the saddle-point versus the uniform approximation. We notice that the saddle-point results exceed the (correct) uniform-

approximation results by about ten percent consistently in the entire region of not too small and not too large momenta p. This may be surprising, since in Fig. 2 discrepancies were minor and restricted to narrow regions of the momentum. The reason is that in the summation over the transverse momenta a Stokes transition, corresponding to a classical cutoff, is encountered for any value of $p_\parallel$. Thus, the spiky artifacts inflate the total yield in the entire classically allowed energy region.

5. CONCLUSIONS

We have addressed the S matrix of nonsequential double ionization in the recollision scenario and in the context of the strong-field approximation. We have analyzed and calculated the transition amplitudes in terms of quantum orbits. This concept is based on a semiclassical evaluation using the saddle-point approximation. It brings about both technical advantages and physical insight. On the technical side, it allows one to deal with arbitrary potentials provided their form factors can be computed in analytical form. This holds both for the binding potential, whose detailed form for fixed binding energy has a comparatively minor effect on the results, and for the effective electron–electron interaction, which is crucial [13]. In the pertinent approach [7–13], the latter is treated in the Born approximation. As for physical insight, the advantage of quantum orbits is that they project a time-dependent picture within the "in–out" formalism of the S matrix, since they allow one to analyze the S matrix in terms of time-dependent orbits, which are closely related to classical electron orbits, and to identify those orbits that lead to the final state of interest. Summing the contributions of many orbits overcomes the limitations of the semiclassical approximation and fully restores quantum-mechanical effects in cases where they are important [22].

The saddle-point approximation treats different saddle points as independent. Therefore, it becomes inapplicable near the boundaries between the classically allowed and forbidden regions, which are characterized by two saddle points approaching each other very closely. In this case, the deficiencies of the saddle-point approximation are healed by the uniform approximation. The latter, moreover, can be used throughout: in the limit of well-separated saddles, it reduces to the former. Furthermore, the uniform approximation is no more complicated than the saddle-point method. Equations (19) and (20) show that it is constructed from the same input: the actions and form factors evaluated at the saddle points.

The saddle points are obtained by solving the saddle-point equations (6) or (25), which give a complex start t for the electron when it leaves the atom and a complex return time t' when it recollides inelastically with its parent ion kicking out the second electron. In the limit where the first ionization potential vanishes and the kinetic energy of the recolliding first electron suffices to free the second electron, the classical equations of motion related to this process are recovered, which have been extensively used to model nonsequential double ionization [26, 27]. In the complex plane, both start and return times exhibit a nonvanishing imaginary part, which increases abruptly as the boundaries of the classically allowed region are reached. For other laser-induced phenomena, such as high-order harmonic generation or above-threshold ionization, this boundary corresponds to the maximal kinetic energy of the returning electron, the so-called cutoff. For nonsequential double ionization, there is also a minimum allowed energy. At such energies, the contribution of one of the saddles starts to diverge and must be discarded. This leads to additional discontinuities in the saddle-point approximation. Within the uniform approximation, this transition occurs smoothly.

The saddle-point equations can be conveniently expressed in terms of longitudinal and transverse electron momenta parallel and perpendicular to the polarization of the external field. The longitudinal momenta, which mark the upper and lower limit of the classically allowed region, depend on the transverse momenta. As a direct consequence, the size of the classically allowed region in $p_\parallel$ depends on the magnitude of the transverse momenta. If the latter are too large, there is no classically allowed region at all. Inside the classically allowed region, the yield is highly oscillating due to interference of the contributions of the two leading quantum orbits; outside of it, the yield decays quickly.

In order to obtain the yield observed in experiments with the observed maxima at nonzero values of the longitudinal momenta, it is necessary to sum over all transverse momenta. This procedure smoothes out the oscillations but, within the saddle-point approximation, introduces a series of artifacts over the entire classically allowed region, which exaggerates the total yield. Using the uniform approximation, this problem is solved, since it is continuously valid over the whole energy region.

The main difference between our approach and the saddle-point computations performed in [11–13] is that, in these references, further approximations are introduced in the computation of the saddle points (t, t'). In fact, in [11–13], the saddle-point equations are expanded in the Keldysh parameter, which is assumed small, and the start and return times are computed semianalytically. Different methods are used [28] to calculate the saddle points away from and near the cutoffs.

The transition amplitude (1) evaluated in this paper and others [7–13] treats the electron–electron interaction in the Born approximation and ignores the interaction between the returning electron and the ion. Replacing the electron–electron Coulomb interaction by a three-body contact potential, as we did in the calculations of this paper, can be interpreted as using an *effective* electron–electron interaction that partly reflects the presence of the ion. However, in any case, the influence

of the ion on the orbit of the first electron between ionization and recollision is left unaccounted for. Hence, there is no Coulomb refocusing, which enhances the NSDI yield by forcing long orbits back towards the ion that would have missed it otherwise [29]. This effect raises the NSDI yield disproportionately for long pulses. All the same, even in the absence of Coulomb refocusing, the long orbits may cause significant enhancements: these are, however, restricted to those intensities that correspond to channel closings [22].

ACKNOWLEDGMENTS

We acknowledge very useful discussions with S.P. Goreslavskii and S.V. Popruzhenko. This work was supported in part by the Deutsche Forschungsgemeinschaft.

REFERENCES

1. Weber, Th., Weckenbrock, M., Staudte, A., *et al.*, 2000, *Phys. Rev. Lett.*, **84**, 443; Weber, Th., Giessen, H., Weckenbrock, M., *et al.*, 2000, *Nature*, **404**, 608; Weckenbrock, M., Hattas, M., Czasch, A., *et al.*, 2001, *J. Phys. B*, **34**, L449.
2. Moshammer, R., Feuerstein, B., Schmitt, W., *et al.*, 2000, *Phys. Rev. Lett.*, **84**, 447; Feuerstein, B., Moshammer, R., Fischer, D., *et al.*, 2001, *Phys. Rev. Lett.*, **87**, 043003; Moshammer, R., Feuerstein, B., Crespo Lopez-Urrutia, J.R., *et al.*, 2002, *Phys. Rev. A*, **65**, 035401.
3. Corkum, P.B., 1993, *Phys. Rev. Lett.*, **71**, 1994.
4. DiMauro, L.F. and Agostini, P., 1995, *Adv. At., Mol., Opt. Phys.*, **35**, 79.
5. Salierés, P., L'Huillier, A., Antoine, Ph., and Lewenstein, M., 1999, *Adv. At., Mol., Opt. Phys.*, **41**, 83.
6. Becker, W., Grasbon, F., Kopold, R., *et al.*, 2002, *Adv. At., Mol., Opt. Phys.*, **48**, 35.
7. Kuchiev, M.Yu., 1995, *J. Phys. B*, **28**, 5093.
8. Becker, A. and Faisal, F.H.M., 1996, *J. Phys. B*, **29**, L197.
9. Becker, A. and Faisal, F.H.M., 2000, *Phys. Rev. Lett.*, **84**, 3546; 2001, *Opt. Express*, **8**, 383.
10. Kopold, R., Becker, W., Rottke, H., and Sandner, W., 2000, *Phys. Rev. Lett.*, **85**, 3781.
11. Popruzhenko, S.V. and Goreslavskii, S.P., 2001, *J. Phys. B*, **34**, L239; Goreslavski, S.P. and Popruzhenko, S.V., 2001, *Opt. Express*, **8**, 395.
12. Goreslavskii, S.P. and Popruzhenko, S.V., 2001, *Super-Intense Laser-Atom Physics*, Piraux, B. and Rzazewski, K., Eds. (Dordrecht: Kluwer), p. 41.
13. Goreslavskii, S.P., Popruzhenko, S.V., Kopold, R., and Becker, W., 2001, *Phys. Rev. A*, **64**, 053402.
14. Keldysh, L.V., 1964, *Zh. Eksp. Teor. Fiz.*, **47**, 1945 [1964, *Sov. Phys. JETP*, **20**, 1307].
15. Lewenstein, M., Balcou, Ph., Ivanov, M.Yu., *et al.*, 1994, *Phys. Rev. A*, **49**, 2117.
16. Salierès, P., Carré, B., Le Déroff, L., *et al.*, 2001, *Science*, **292**, 902.
17. Kopold, R., Becker, W., and Kleber, M., 2000, *Opt. Commun.*, **179**, 39.
18. Bleistein, N. and Handelsman, R.A., 1986, *Asymptotic Expansions of Integrals* (New York: Dover).
19. Berry, M.V., 1989, *Proc. R. Soc. London, Ser. A*, **422**, 7.
20. Schomerus, H. and Sieber, M., 1997, *J. Phys. A*, **30**, 4537.
21. Figueira de Morisson Faria, C., Schomerus, H., and Becker, W., 2002, *Phys. Rev. A* **66**, 043413.
22. Popruzhenko, S.V., Korneev, Ph.A., Goreslavski, S.P., and Becker, W., 2002, *Phys. Rev. Lett.*, **89**, 023001.
23. Panfili, R., Haan, S.L., and Eberly, J.H., 2002, *Phys. Rev. Lett.*, **89**, 113001.
24. van der Hart, H.W. and Burnett, K., 2000, *Phys. Rev. A*, **62**, 013407.
25. Cohen, J.S., 2001, *Phys. Rev. A*, **64**, 043412.
26. Feuerstein, B., Moshammer, R., and Ullrich, J., 2000, *J. Phys. B*, **33**, L823.
27. Chen, J., Liu, J., Fu, L.B., and Zheng, W.M., 2001, *Phys. Rev. A*, **63**, 011404(R).
28. Goreslavskii, S.P. and Popruzhenko, S.V., 1999, *J. Phys. B*, **32**, L531; 2000, *Laser Phys.*, **10**, 583.
29. Bhardwaj, V.R., Aseyev, S.A., Mehendale, M., *et al.*, 2000, *Phys. Rev. Lett.*, **86**, 3522; Yudin, G.L. and Ivanov, M.Yu., 2001, *Phys. Rev. A*, **63**, 033404.